

Defect Engineering of Copper Paddlewheel-Based Metal–Organic Frameworks of Type NOTT-100: Implementing Truncated Linkers and Its Effect on Catalytic Properties

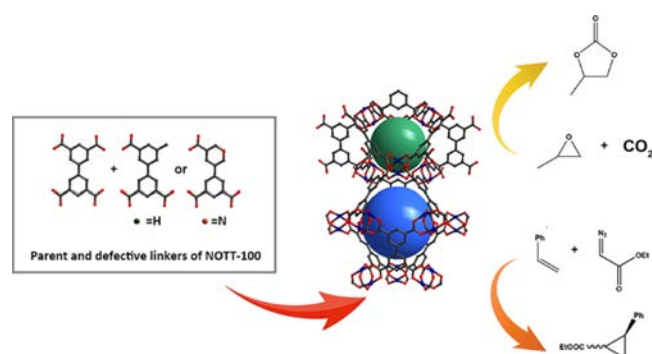
Zhiying Fan, Junjun Wang, Weijia Wang, Stefan Burger, Zheng Wang, Yuemin Wang, Christof Wöll, Mirza Cokoja, and Roland A. Fischer*

ABSTRACT: A series of new defect engineered metal–organic frameworks (DEMOFs) were synthesized by framework doping with truncated linkers employing the mixed linker approach. Two tritopic defective (truncated) linkers, biphenyl 3,3',5 tricarboxylates (L_H) lacking a ligating group and 5 (5 carboxypyridin 3 yl)isophthalates (L_{Py}) bearing a weaker interacting ligator site, were integrated into the framework of Cu_2 (BPTC) (NOTT 100, BPTC = biphenyl 3,3',5,5' tetracarboxylates). Incorporating L_H into the framework mainly generates missing metal node defects, thereby obtaining dangling COOH groups in the framework. However, introducing L_{Py} forms more modified metal nodes featuring reduced and more accessible Cu sites. In comparison with the pristine NOTT 100, the defect engineered NOTT 100 (DE NOTT 100) samples show two unique features: (i) functional groups (the protonated carboxylate groups as the Brønsted acid sites or the pyridyl N atoms as the Lewis basic sites), which can act as second active sites, are incorporated into the MOF frameworks, and (ii) more modified paddlewheels, which provided extra coordinatively unsaturated sites, are generated. The cooperative functioning of the above characteristics enhances the catalytic performance of certain types of reactions. For a proof of concept, two exemplary reactions, namely, the cycloaddition of CO_2 with propylene oxide to propylene carbonate and the cyclopropanation of styrene, were carried out to evaluate the catalytic activities of those DE NOTT 100 materials depending on the defect structure.

KEYWORDS: defect engineering, metal–organic frameworks, heterogeneous catalysis, mixed linker, NOTT 100

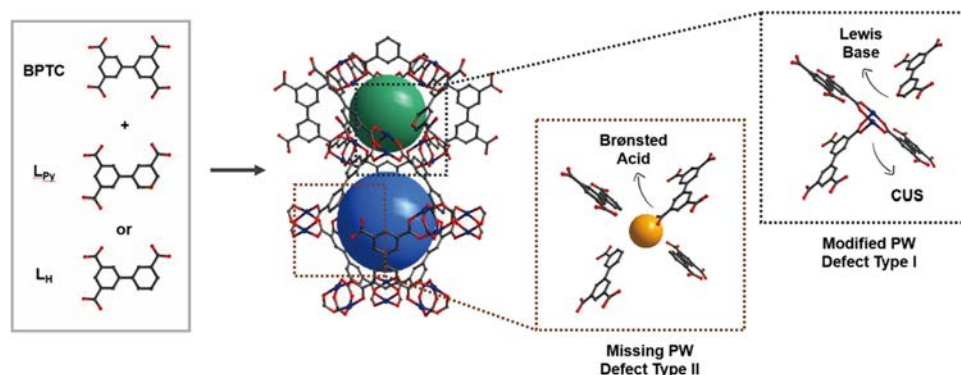
1. INTRODUCTION

Owing to the controllable composition, for instance, the diversified framework architectures and high surface areas, metal–organic frameworks (MOFs) have continuously been attracting intense research interest for various applications such as gas storage/separation,^{1–6} heterogeneous catalysis,^{7–13} and drug delivery.^{14,15} The chemical and physical properties of MOFs can be finely tailored by choosing different organic linkers (L) and secondary building units (SBUs). The postsynthetic modification and pre installation of ligands with functionalized side chains have become effective methods to tune the properties of the frameworks to achieve the desired features.^{16–20} However, it was found that modifications of linkers with pending side groups or other functionalizations (grafting) resulted in a significant reduction in the specific surface area and increase in diffusion limitation, which may be undesirable for various practical applications, especially for catalysis.²⁰ The catalytic properties of MOFs mainly depend on their compositions and structure. If we only focus on the



MOF itself and do not consider hybridizing MOFs with catalytically active guests such as metal nanoparticles, etc., then there are two conceptual methods to improve the intrinsic MOF catalytic properties: (i) introducing functional linkers with catalytically active sites into the MOF framework and (ii) changing the local coordination environments of the metal nodes to obtain more accessible and catalytically active metal sites. The majority of MOFs feature coordinatively saturated or sterically shielded metal sites that are not accessible as reaction centers for catalysis. One approach to manipulate the properties of MOFs is to introduce defects into the targeted frameworks by mixing the pristine linker with its fragmented

Scheme 1. Schematic Illustration of Defect Creation in NOTT 100 by Mixed Linker Approach and Conceptual Structure of the Two Types of Paddlewheel Related Defects^a



^aColor codes of the atoms: Cu, blue; C, gray; O, red; N, brown. CUS: coordinatively unsaturated site.

derivatives (i.e., defect generating truncated linkers with different functionalities and weaker coordinating groups).^{21–24}

Two main perspectives of this method can be listed as follows: (i) The surface and internal structure of MOFs can be functionalized but limit or even avoid the reduction of the pore volume and pore size. Even enhancing the accessible surface area and the design of hierarchical (micro/meso) porosity is possible. (ii) The local coordination environments of the metal centers at the nodes (SBUs) can be changed around the defect sites, thereby affecting the chemical and structural properties of MOFs.^{25,26}

Recently, there is a great interest in the targeted synthesis of defect rich MOFs and their use for practical purposes.^{27–30}

Despite the progress, using Cu sites in defect engineered Cu MOFs (DE Cu MOFs) as active centers to catalyze organic reactions is very rare.^{31,32} Baiker et al. partially replaced the benzene 1,3,5 tricarboxylate (BTC) linker by pyridine 3,5 dicarboxylate (PyDC) in $\text{Cu}_3(\text{BTC})_2$ (HKUST 1), which resulted in changes of the electronic structure and the catalytic properties of the modified MOFs.³¹ The obtained defective $\text{Cu}_3(\text{BTC})_2$ MOFs could catalyze the hydroxylation of toluene and show different selectivity toward various oxidation products. Schröder et al. prepared a series of mesoporous DE Cu MOFs containing crystal defects by a new templated electrosynthesis approach and found that they exhibit very high activity and selectivity for aerobic oxidation of alcohols to aldehydes.³² For the above mentioned DE Cu MOF materials, the researchers were committed to creating more Lewis acid sites to improve their catalytic activities. However, no DE Cu MOFs have been used for the Cu catalyzed reactions so far. Furthermore, none of the aforementioned studies specifically discussed how to tailor the overall defect structure and thus the properties of MOFs through the design of defect generating ligands. In our previous works, we introduced a series of defect generating linkers into HKUST 1 analogs (Cu and Ru) to form the respective defect engineered MOFs (DE MOFs).^{21,33–35} In the frameworks, two kinds of structural defects were discovered: (i) modified paddlewheels featuring a lowered coordination number of the metal sites accompanied with reduced oxidation states (type I) and (ii) missing paddlewheel defects (type II). In the case of type II defects, uncoordinated carboxylic acid groups could be present and point toward the missing node area in the framework. Since MOFs with different types of defects exhibit different modulated properties (e.g., better or altered catalytic activity

or higher porosity compared to the pristine one), it is important to understand the nature and formation of different kinds of defects in MOFs by this approach of integrating defect generating linkers to the framework.

In this work, we transferred our knowledge of the 3,4 connected HKUST 1 into the 4,4 connected NOTT 100 to further study structural complexity in DEMOFs. In the known literature, pristine NOTT 100 was constructed from Cu PWs and biphenyl 3,3',5,5' tetracarboxylates (BPTC) with NbO topologies, which have been examined as potential adsorbents for H_2 and CH_4 .^{36–38} Two asymmetric tritopic defective linkers of similar topology as the parent BPTC, biphenyl 3,3',5 tricarboxylates (L_H) lacking one ligating carboxylate group and 5 (5 carboxypyridin 3 yl)isophthalates (L_Py) bearing one weaker interacting pyridyl type ligator site, were integrated into defect engineered NOTT 100 (DE NOTT 100) via the mixed linker approach (Scheme 1). The influence of these two different defect generating linkers L_H and L_Py on the patterns of type I/type II defect formation was carefully investigated on a selection of samples (DE NOTT 100 MOFs), utilizing PXRD, ^1H NMR spectroscopy, ultrahigh vacuum IR spectroscopy, XPS, and N_2 sorption. Notably, the generation of more CUSs within the NOTT 100 framework has endowed the resultant DE NOTT 100 MOFs with higher activity for the Cu catalyzed cyclopropanation of styrene. In addition, we also selected the cycloaddition of CO_2 with propylene oxide as the exemplary reaction to evaluate the improvement of the catalytic performance of DE NOTT 100 MOFs by introducing catalytically active, functional groups.

2. EXPERIMENTAL SECTION

2.1. Materials. BPTC and L_H were synthesized according to previously reported procedures.^{39,40} All chemicals for MOFs synthesis and catalytic reactions were purchased from commercial suppliers and used without further purification. All dried defect engineered MOFs (DEMOFs) were stored under argon in a glove box.

2.2. General Methods. Powder X ray diffraction measurements were performed using Bragg–Brentano geometry in a PANalytical Empyrean diffractometer equipped with a PANalytical PIXcel 1D detector. The measurement was performed at 298 K and the activated sample was filled into a capillary (0.5 mm) and rotated on a reflection transmission spinner during the measurement (0.5 rps). For selected PXRD patterns, a Pawley profile fit analysis was carried out by using TOPAS Academic v6 operated in GUI mode using input files. Standard deviations of all parameters were calculated and with the use of “randomize on errors”, it was ensured that the minimum of

refinement was achieved.^{41,42} Gas physisorption measurements were performed on a Micromeritics 3Flex surface analyzer. The ¹H NMR spectra were recorded on a Bruker AV400US spectrometer at 400 MHz. The FTIR spectra of the activated samples were collected under argon by a Bruker Alpha P FTIR spectrometer (from 4000 to 400 cm⁻¹) using a diamond attenuated total reflection (ATR) unit. Thermal gravimetric analysis (TG) of materials was carried out using a Mettler Toledo TGA/DSC 3+ MS instrument at atmospheric pressure under flowing syn air and a heating rate of ~10 K min⁻¹ in a temperature range from 303 to 873 K. Ultrahigh vacuum (UHV) FTIR measurements were conducted with a novel UHV FTIR apparatus. The powder samples were first pressed into a stainless steel grid covered by gold and then mounted on a sample holder, which was specially designed for the FTIR transmission measurements under UHV conditions. The grid was cleaned by heating up to 850 K to remove all contaminants formed on it during the preparation. The base pressure in the measurement chamber was 5 × 10⁻¹⁰ mbar. The optical path inside the IR spectrometer and the space between the spectrometer and UHV chamber were also evacuated to avoid atmospheric moisture adsorption, resulting in high sensitivity and stability. The DEMOF samples were cleaned in the UHV chamber by heating to 430 K to remove the contaminants involved during synthesis and all the adsorbed species such as water and hydroxyl groups. Prior to each exposure, a spectrum of the clean sample was recorded as a background reference. The exposure of the sample to CO was carried out by backfilling the measurement chamber through a leak valve. High resolution X ray photoelectron spectroscopy (XPS) measurements were carried out in a UHV setup equipped with a high resolution RG Scienta 4000 analyzer.

2.3. Preparation of L_{py}. *n* Butyllithium (1.6 M in hexane, 4.7 mL) was added dropwise to a solution of 3 bromo 5 methylpyridine (1.07 g) and triisopropylborate (1.87 mL) in anhydrous diethyl ether (Et₂O, 40 mL) at 195 K. The reaction mixture was stirred for 20 min at 195 K, and then the temperature was increased to RT in 2 h. After that, the mixture was stirred overnight and treated with H₂O (10 mL). The organic phase was extracted with 0.5 N NaOH, washed with Et₂O, and then acidified with 2 N HCl to pH 6. The white precipitate (5 methylpyridin 3 yl)boronic acid was collected by filtration. The obtained heteroarylboronic acid (814 mg), [Pd₂(dba)₃] (46 mg), and PCy₃ (34 mg) were added to a 25 mL Schlenk flask equipped with a stir bar in an argon atmosphere. Dioxane (13.5 mL), 1 bromo 3,5 dimethylbenzene (680 mL), and K₃PO₄ (1.8 g) in 6.65 mL of H₂O were added using a syringe. The Schlenk flask was sealed and heated in an oil bath at 373 K for 18 h with vigorous stirring. The mixture was concentrated and purified by column chromatography on silica gel. Then, the obtained 3 (3,5 dimethylphenyl) 5 methylpyridine was oxidized to L_{py} using KMnO₄ in *tert* butanol/water (1:1, v/v) containing NaOH. ¹H NMR (DMSO *d*₆, 400 MHz): 9.14 (d, 1H), 9.10 (d, 1H), 8.50 (t, 1H), 8.48 (t, 1H), 8.43 (d, 2H). ¹³C NMR (DMSO *d*₆, 400 MHz): 166.76, 166.52, 151.70, 150.09, 137.55, 135.40, 134.42, 132.87, 132.08, 130.18, 127.41.

2.4. MOF Synthesis. Pristine NOTT 100 was prepared following the reported method.³⁷ The DEMOFs H1–H4 and Py1–Py3 were synthesized by using analogous procedures with slight modification. Cu(NO₃)₂·3H₂O (0.86 mmol, 208 mg) was dissolved in H₂O/dioxane (15 mL, 1:1 v/v), and ligands of L_H or L_{py} (*n* mmol) and BPTC (0.344 – *n* mmol) were dissolved in 15 mL of DMF. Then, the obtained solutions were combined in a sealed bottle and mixed with HCl (37%, 86 μL), and then the mixture was heated at 80 °C for 3 days. The as synthesized materials were collected by centrifugation, washed with DMF to remove residual precursor species, and then dried in air. The samples were guest exchanged with dry acetone and activated for 15 h (H1–H4 at 120 °C and Py1–Py3 at 150 °C).

2.5. Catalytic Reactions. **2.5.1. CO₂ Cycloaddition.** The cocatalyst TBAB (10 mol %) together with MOFs (0.5 mol %, calculated based on copper paddlewheel unit) was put into a Fischer Porter bottle in an argon filled glove box. Then, propylene oxide (10 mmol) was added, and the reactor was pressurized with ca. 2 bar CO₂. The solution was stirred at 328 K for 48 h. The yields were calculated

based on ¹H NMR analysis. The recovered catalyst was collected by centrifugation, washed by fresh ethanol, and dried in vacuum.

2.5.2. Cyclopropanation Reaction. The MOF catalysts (5 mol %, calculated based on copper paddlewheel unit) and styrene (2.4 mmol) were suspended in 2 mL of dichloromethane (DCM), and 0.24 mmol of ethyl diazoacetate (EDA) in 1 mL of DCM was added with a syringe pump over 2 h. The resulting mixture was stirred at room temperature. The reaction was monitored by gas chromatography (GC). The recovered catalyst was collected by centrifugation, washed by fresh ethanol, and dried in vacuum.

3. RESULTS AND DISCUSSION

3.1. Structure, Composition, and Porosity of DE-NOTT-100 MOFs. Two kinds of defective linkers (L_H and L_{py}) were incorporated into the pristine NOTT 100 framework. All those variants (H1–H4 and Py1–Py3) are isostructural to the pristine NOTT 100 and were obtained by mixing the pristine linker (BPTC) with different molar ratios of the defective linker L_H or L_{py} via the solvothermal synthesis method. The sample naming scheme is based on the defect generating linker types and the doping degrees of framework incorporated defective linkers (Table S1 in the Supporting Information). The crystal structures and crystal linity of the obtained MOFs were investigated via powder X ray diffraction (PXRD). It was found that more than 50 mol % (with respect to total linker concentration) of BPTC can be replaced by defective linkers without affecting the network topology (Figure 1). We selected Py2 as the represented

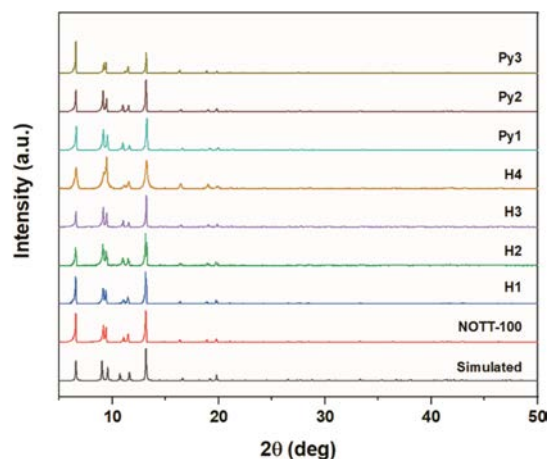


Figure 1. PXRD patterns of simulated NOTT 100, pristine NOTT 100, and as synthesized DE NOTT 100 samples (H1–H4 and Py1–Py3). All the samples are activated.

sample to confirm the phase purity of the material. A Pawley profile fit analysis of the powder pattern was carried out and all the appearing reflections could be assigned to the respective unit cell, confirming the crystal structure of NOTT 100, which was originally reported (Figure S1).³⁶ As a refined unit cell for the as synthesized MOF at room temperature, we found unit cell parameters of *a* = 18.482753 Å, *c* = 24.935978 Å, and *V* = 7377.180 Å³ in the trigonal setting (with hexagonal axes) with space group *R* 3*m* (see Supporting Information for details). Upon activation of Py2, we observed a slight reduction of unit cell volume to *V* = 7194.081 Å³, which is well known and characteristic for this MOF material class.⁴³ Thermogravimetric analysis (TGA) data show that the thermal stability of all DE NOTT 100 samples is only slightly lower than that of the original NOTT 100 (Figure S2). This is consistent with

previous observations that the overall stability of MOF samples is reduced upon the incorporation of defects.^{43–46} Note that defect engineering of HKUST 1 by replacing the tritopic BTC linker with functionalized ditopic isophthalate linkers leads to a more pronounced reduction of the thermal stability by defective linker incorporation.²¹

To determine the presence and amount of framework incorporated defective linkers within the structure, the ¹H NMR spectra were recorded using carefully purified (washed), activated, and then quantitatively digested samples (Figure S3). The results were achieved by following a previously reported procedure with slight modifications.⁴⁷ A certain amount of activated samples were digested in basic conditions within NaOD/D₂O, and the mixtures were heated. During this process, the organic linkers in the frameworks were dissolved, and metallic contents (Cu) were transformed into a black solid, which could be filtered off. The shielding effect of the paramagnetic cupric ions on NMR is excluded by this base digested procedure. The ratios of the amount of defective linkers to that of total linkers in the obtained materials were calculated and are presented in Table S1. Interestingly, when an equal amount of defective linker is fed, the L_{Py} is more incorporated into the framework compared with the L_H. This finding indicates that the doping ratios of defective linkers/total linkers in the frameworks strongly depend on the nature of the defective linkers, and L_{Py} bearing weaker interacting ligand sites is more likely to be incorporated in the structure. Note that, in general, there is no predictable quantitative correlation between the feeding ratio and framework incorporation fraction of defective linkers with respect to the parent one as a function of the type of linkers and framework. This is also true for the general synthesis of mixed linker MOFs by solvothermal methods.^{21,31,35}

To determine the permanent porosity of the prepared (activated) samples, N₂ adsorption isotherms (77 K) were measured (Figure 2). All of the samples retain a high specific surface area while maintaining a type I adsorption isotherm, indicating that the introduction of defective linkers into NOTT 100 does not damage its structure. The samples H1–H3 result in almost the same nitrogen uptake as that of pristine NOTT 100, which provides evidence that L_H is incorporated in the MOF framework rather than occupying the pores. However, a further increase in the L_H content leads to a decrease in the surface area of H4. When excessive L_H is introduced, the high abundance of the defective linkers with only three carboxylate ligand sites is unable to support the self-assembly of the entire framework, which obviously leads to the collapse of some pores. The BET surface areas for Py1 and Py2 are slightly higher than that of pristine NOTT 100. Similar to the L_H case, when the doping ratio of L_{Py} reaches 50 mol %, the surface area of the obtained sample decreases. However, the N₂ uptake of Py3 is still comparable to that of the pristine NOTT 100. The CO₂ adsorption isotherms (298 K) of Py1–Py3 were also measured, and they follow the same trend of N₂ uptakes (Figure 2b, inset). The pore size distribution (PSD) of the pristine and defect engineered MOFs was also provided (Figure S4). Figure S4a shows that the dominant micropores in pristine NOTT 100 are centered at around 6.1 and 6.8 Å. After integrating defect generating linkers, pores with larger sizes were formed. No obvious change could be found in PSD of Py1 and H1 because only 10 and 7% defective ligands were introduced into their framework, respectively. When the doping levels gradually increase, Py2 and Py3 show an

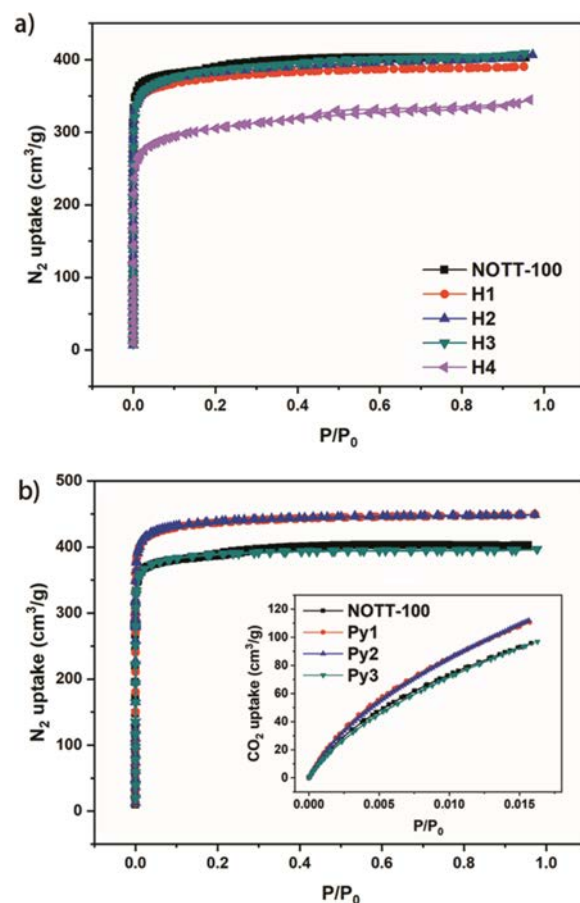


Figure 2. (a) N₂ adsorption isotherms of pristine NOTT 100 compared to H1–H4. (b) N₂ adsorption isotherms at 77 K and CO₂ adsorption isotherms at 298 K (inset) of pristine NOTT 100 and Py1–Py3.

additional peak at 10.9 Å. In addition, H2–H4 also exhibit a new peak at a larger width (about 19.5 Å). In most traditional functionalization methods, functional groups occupy the pores and cause a reduction in specific surface area and pore size. In contrast, samples prepared by the “defect generating linker method” have comparable or even increased surface areas with various functionalities provided by the defective linker.

3.2. Probing Oxidation States of Cu Sites and Defect Types in DE-NOTT-100 MOFs. In following previous work,^{21,35} the type of metal site and, in particular, the concentration of Cu¹⁺ CUSs were determined by employing the CO SLIR (surface ligand IR spectroscopy) approach.^{48–51} The generation of type I defects was proposed (modified PW with three BTC linkers and one PyDC linker, in which the pyridyl N site acted as a weak ligating site toward the Cu PW). Since PyDC has one less charge than BTC and other charge compensating anions are absent, Cu²⁺ is chemically reduced to Cu¹⁺ to balance the charge in the course of the solvothermal synthesis. However, when 5 isophthalate (ip) was doped into HKUST 1, much fewer Cu¹⁺/Cu²⁺ PWs were generated. It was explained by the formation of type II defects where the entire Cu²⁺/Cu²⁺ PW is missing. Note that, also in the case of PyDC, such type II defects may be present. These results revealed that different types of defects could be created in a controlled fashion by choice of defect generating ligands in a specific type of MOF structure.

In this work, we chose NOTT 100, which is also based on Cu paddlewheel building blocks, as a model material to further study different types of defects. Two kinds of asymmetric tritopic defective linkers (L_H lacking a ligating group and L_{Py} bearing weaker interacting ligator sites) were designed and integrated into the framework of NOTT 100. We speculated that due to the tetratopic nature of the parent BPTC and the essentially tritopic nature of L_H and L_{Py} , the selectivity toward the formation of type I defects should be enhanced.

To characterize the local chemical environments of metal paddlewheel nodes in the pristine and defect engineered NOTT 100 MOFs, in situ UHV FTIRS measurement utilizing CO as the probe was employed on representative samples. Our previous IR results acquired for DE HKUST 1 allow for a reliable assignment of the spectroscopic features. The corresponding IR spectra of pristine NOTT 100, H3, and Py2 are presented in Figure 3. The observed CO vibrational bands and their assignments are summarized in Table 1.

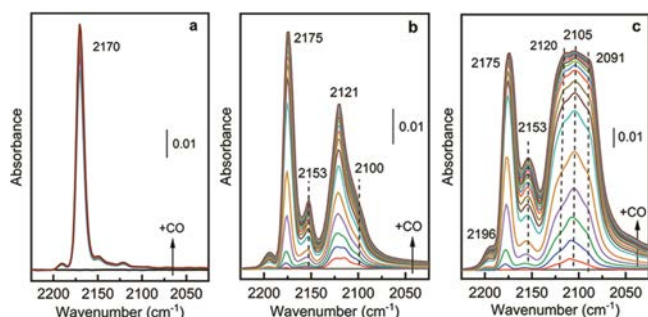


Figure 3. UHV FTIRS data obtained after CO adsorption (0.01 mbar) on pristine and defect engineered NOTT 100 MOFs at 100 K. (a) Pristine NOTT 100; (b) H3; (c) Py2. Before CO adsorption, the MOF samples were heated in UHV at 430 K.

Table 1. Vibrational Frequencies and Assignment of Various CO Species Adsorbed on Pristine NOTT 100 and DE NOTT 100 (H3 and Py2) Samples

sample	CO vibration (cm^{-1})	assignment
pristine NOTT-100	2170	CO- Cu^{2+}
H3	2175	CO- Cu^{2+}
	2121, 2100	CO- Cu^{1+}
	2153	$(\text{CO})_2\text{-Cu}^{1+}$
Py2	2175	CO- Cu^{2+}
	2120, 2105, 2091	CO- Cu^{1+}
	2153	$(\text{CO})_2\text{-Cu}^{1+}$
	2196	$(\text{CO})_2\text{-Cu}^{2+}$

For the pristine NOTT 100 (Figure 3a), one intense band appears at 2170 cm^{-1} being characteristic for CO adsorbed to Cu^{2+} CUS, while the CO Cu^{1+} related vibrations are detected only as extremely weak signals at the lower frequency region. This finding provides direct evidence for the formation of nearly defect free NOTT 100. Indeed, the corresponding Cu 2p XPS results show a very low concentration (2%) of Cu^{1+} species (see Figure S5). The presence of reduced Cu^{1+} sites in the pristine sample is most likely due to intrinsic defects generated during the synthesis of NOTT 100 as it is well known for HKUST 1.

For DE NOTT 100 MOFs (H3 and Py2, see Figure 3b,c), numerous CO bands between 2090 and 2130 cm^{-1} show up along with the introduction of different defective linkers. These

IR bands are ascribed to various CO species bound to modified Cu^{1+} CUSs with rather different electronic and steric properties with respect to the intact $\text{Cu}^{2+}/\text{Cu}^{2+}$ PWs (Table 1).²¹ The relative intensity of the Cu^{1+} related CO bands increases significantly compared to that of the pristine NOTT 100, confirming the generation of type I defects, i.e., reduced $\text{Cu}^{1+}/\text{Cu}^{2+}$ PWs. The $\text{Cu}^{1+}/\text{Cu}^{2+}$ CUS dimers with lowered coordination numbers expose an additional open space. Accordingly, a second CO can adsorb to the copper site.⁵¹ This is supported by the observation of weak IR bands at 2153 and 2196 cm^{-1} (Figure 3b,c), which are attributed to the asymmetric stretch vibration of geminal $(\text{CO})_2\text{Cu}^{1+}$ and $(\text{CO})_2\text{Cu}^{2+}$ species, respectively.^{49,50,52,53}

Importantly, H3 and Py2 were prepared with quite comparable doping levels (framework incorporation of about 33% L_H for H3 and about 30% L_{Py} for Py2) of different defective linkers; however, the relative intensity of Cu^{1+} related IR bands of Py2 (Figure 3c) is much higher than that of H3 (Figure 3b). Furthermore, on the basis of a quantitative analysis of the XPS data (Figure S5), the concentration of Cu^{1+} species was determined to be significantly higher in Py2 (29%) than that in H3 (18%), in excellent agreement with the IR observation. These results reveal the presence of more type II defects (i.e., missing metal nodes) in H3 than in Py2. This finding is attributed to the weak ligand-metal interaction between Cu sites and the pyridyl N donors of L_{Py} , thereby reducing or even avoiding the generation of missing paddlewheel defects.

Furthermore, we used ATR FTIR spectroscopy to elucidate the structure of the MOFs and present the results in Figure 4. Interestingly, The H1-H4 show an additional peak at $\sim 1700 \text{ cm}^{-1}$ compared with pristine NOTT 100, which can be assigned to $\nu(\text{C}=\text{O})$ from uncoordinated carboxylate groups.⁵⁴⁻⁵⁶ However, this peak is not observed in Py1-Py3. We further use CO as the probe molecule to probe the density of Brønsted acid sites. CO binds to Brønsted acid OH sites, leading to frequency shifts of the OH as well as of the CO stretch vibration. This method is well suited for MOFs.⁵⁷ Increasing acidity leads to a decrease in the OH frequency and an increase in the CO stretch frequency.⁵⁸ In the Supporting Information, we present IR results (Figure S6) recorded for different DE NOTT 100 samples. After exposing H3 to CO at 100 K, the OH band at 3502 cm^{-1} , which is characteristic for protonated carboxylic acids, shows clearly a CO induced red shift to 3484 cm^{-1} (see Figure S6a).⁵⁹ Importantly, such CO induced shifts of OH vibrational bands were not observed for the DE NOTT 100 samples modified by the L_{Py} defective linkers (Py2, see Figure S6b), revealing that the density of acidic OH sites is much lower in these samples. These results clearly reveal that only the framework incorporation of L_H but not L_{Py} leads to the formation of Brønsted acid sites in DE NOTT 100 MOFs. The most likely cause is the formation of more missing paddlewheel defects (type II defects) in H1-H4. As shown in Scheme 1, uncoordinated carboxylic acid groups could be present and point toward the missing node area in the framework. The formation of more missing metal node defects can lead to the creation of more vacancies (larger pores), which is in agreement with the PSD results (Figure S4). The relatively high abundance of type II defects can lead to the collapse of some pores, thereby reducing the specific surface area. This is also consistent with the BET results (Figure 2 and Table S2). Therefore, the choice of defect generating ligands is

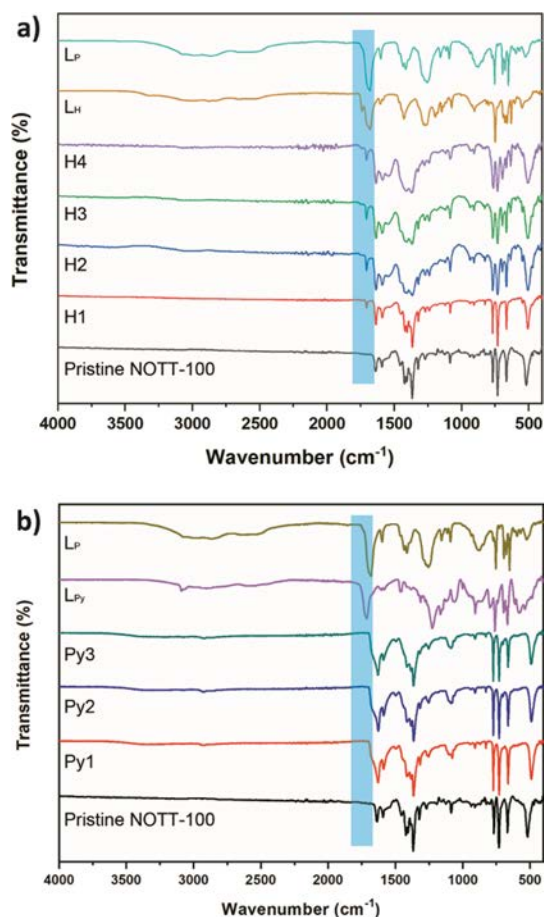


Figure 4. IR spectra of (a) H1–H4 and (b) Py1–Py3 (all MOF samples are activated). For comparison, the IR spectra of BPTC, L_H , and L_{Py} are also shown.

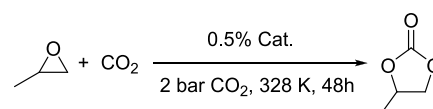
expected to play a critical role in the formation of different types of defects in the NOTT 100 system.

3.3. Catalytic Test Reactions. Compositions and structures of MOF frameworks can strongly influence their catalytic performance. In this work, we manipulated the composition and structure of NOTT 100 to create, expose, and modify more catalytic sites, thereby improving its catalytic performance. Compared with the pristine NOTT 100, DE NOTT 100 with L_{Py} and L_H as defective ligands both showed better catalytic performance, but the catalytic activities of these DE NOTT 100 MOFs come from different structural characteristics. In the case of L_H as the defective linker, due to the lack of a ligating group in L_H , type II defects are more dominant in the resulting DEMOFs (H1–H4), resulting in the presence of Brønsted acid sites originating from uncoordinated carboxylic acid groups. In the case of L_{Py} as the defective linker, type I defects are mainly generated since the pyridyl N of L_{Py} has a weak ligand–metal interaction with Cu sites. Therefore, Lewis basic sites and more CUSs are incorporated into Py1–Py3. To evaluate the catalytic activities of the obtained defective materials, cycloaddition of CO_2 with propylene oxide to propylene carbonate and the cyclopropanation of styrene were selected in this work.

3.3.1. Cycloaddition of CO_2 and Propylene Oxide to Propylene Carbonate. The cycloaddition reaction of CO_2 and epoxides to cyclic carbonates is one of the best studied catalytic reactions involving CO_2 as the reactant.^{60–63}

Generally, an MOF is used with a Lewis basic cocatalyst to catalyze this reaction. The epoxide is activated by the open metal coordination sites (acting as Lewis acid sites) of MOFs and then ring opened by the nucleophilic species provided by the cocatalysts.⁶⁴ The Cu PW based MOFs have recently been shown to exhibit excellent activity and/or selectivity toward this kind of reaction.^{65–67} Therefore, the cycloaddition of CO_2 and propylene oxide is investigated to show how incorporating defect generating linkers influences the catalytic properties of DE NOTT 100 MOFs. Since the Cu at the defect site (type I) is less hindered and Lewis basic pyridyl sites can promote this reaction,^{68,69} we assumed that the Py1–Py3 should have higher catalytic activities for this kind of reaction. As expected, all of them exhibit better performance for the cycloaddition of CO_2 and propylene oxide to propylene carbonate in comparison with that of the pristine NOTT 100. As shown in Table 2, the conversions of propylene (Py1 and Py2)

Table 2. Cycloaddition of CO_2 and Propylene Oxide Catalyzed by Different MOF Materials and Cu Salts^a



entry	catalyst	conversion (%) ^b
1	NOTT-100	66
2	Py1	81
3	Py2	96
4	Py3	91
5	H3	90
6	Cu(OAc)	27
7	Cu(OAc) ₂	94 ^c

^aReaction condition: propylene oxide (10 mmol), TBAB (10 mol %), MOF (0.5 mol %, calculated based on Cu content), 2 bar CO_2 , 328 K, and 48 h. ^bDetermined by ¹H NMR spectroscopy. ^cReaction time: 24 h.

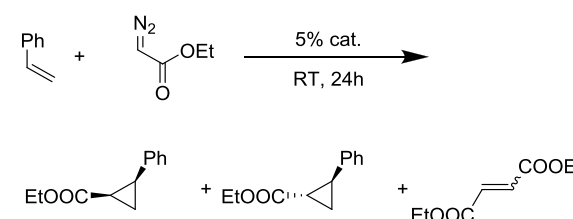
increase with the increasing degree of incorporation of L_{Py} . However, the further increase in the L_{Py} content results in a slight decrease in the catalytic activity, which can be explained by the reduced crystallinity and slightly lower CO_2 uptake. Moreover, it is worth noting that the extra Cu^{1+} sites exposed in the modified PWs are not typical Lewis acid sites for catalyzing the cycloaddition reaction. Under the same condition, the catalytic activity of such a kind of soft Lewis acid Cu^{1+} site is extremely low for this reaction (Table 2, entry 6), which eliminated the possibility that those cuprous sites could serve as active sites. We also tested materials H3 (33% L_H) as catalysts in the selected reaction and obtained a similar yield to Py2 (30% L_{Py}). However, unlike py2, the increased activity of H3 is due to the Brønsted acid sites originating from dangling protonated carboxylic acid groups.^{55,70}

We selected Py2 as the representative sample to confirm the recyclability of the DE NOTT 100 MOFs in the cycloaddition of CO_2 reaction. The Py2 can be reused at least four catalytic cycles without obvious degradation in catalytic activity (Figure S7). Upon recovery of Py2 after the CO_2 cycloaddition reaction as well as reactivation of the MOF material, we found some marginal changes in the PXRD patterns (Figure S8). Pawley profile fit analysis of these samples confirms retaining of the crystal structure of the pristine Py2 as all reflections could still be assigned to the space group $R\bar{3}m$ and the same

unit cell dimensions without observation of any new signals despite some loss of crystallinity through these steps, resulting in small broadening and thus partial overlap of the Bragg peaks and some decrease in total counts (Figure S9). Note that some of the very adjacent reflections visualized in Figure S9a partially overlap in Figure S9b due to peak broadening but still could be assigned as two reflections during fitting.

3.3.2. Cyclopropanation of Styrene. Transition metal catalyzed carbene transfer from diazo derivatives to olefins is a powerful method to give cyclopropane rings.^{71–74} Iglesias and co workers prepared two imine linked polymer–organic frameworks (POFs) and modified them with Cu by postsynthetic metalation.⁷⁵ They compared the catalytic activity of both Cu¹⁺ and Cu²⁺ based POFs for the cyclopropanation of alkenes and found that the Cu¹⁺ modified material had higher activity. These results are consistent with earlier observations that Cu¹⁺ species are catalytically active in the carbene transfer with diazo compounds and that Cu²⁺ species are reduced to Cu¹⁺ species first by the diazo compounds before the carbene transfer reaction.⁷⁶ Having more Cu open metal sites in the DE NOTT 100 MOFs, materials Py1–Py3 were employed as catalysts in the cyclopropanation of styrene with ethyl diazoacetate (EDA). Pristine NOTT 100 was used as a reference material. In Table 3, the DE NOTT 100 MOFs containing L_{py} as a defective

Table 3. Cyclopropanation of Styrene and EDA Catalyzed by Different MOF Materials^a



entry	catalyst	conversion (%) ^b	cis:trans
1	NOTT-100	23	1:2
2	Py1	45	1:2
3	Py2	98	1:2
4	Py2	11 ^c	1:2
5	Py3	63	1:2
6	H3	100 ^c	1:2

^aReaction condition: styrene (2.4 mmol), EDA (0.24 mmol), MOF (5 mol %, calculated based on Cu content), room temperature, and 24 h. GC–MS analyses show that about 10% of EDA self coupling products were formed together with desired cyclopropane derivatives.

^bDetermined by GC FID. ^cReaction time: 4 h.

linker are more active than pristine NOTT 100 to this reaction. Among all tested samples, Py2 shows the highest catalytic activity. The conversion of EDA reaches 98% in 24 h when employing Py2 as the catalyst, much higher than that for pristine NOTT 100 (23%) under the identical condition. These can be attributed to the generation of more accessible Cu sites (type I defects) in DE NOTT 100 MOFs containing L_{py}. We also used H3 (33% L_H) as the catalyst in the cyclopropanation reaction under the same condition. Interestingly, the activity of H3 is much higher than that of Py2. The conversion of EDA reaches 100% within 4 h when using H3 as the catalyst while only 11% for Py2 at the same time. This is most presumably a consequence of the presence of Brønsted acid sites in H3. It is known that the rate limiting step of the

cyclopropanation reaction is the formation of copper carbene intermediate via metal mediated decomposition of diazo compounds.⁷⁷ In addition to transition metals, Brønsted acids can also promote the activation of diazo compounds^{78,79} and then greatly accelerate the reaction.

H3 was selected as the representative sample to investigate the reusable efficiency of the DE NOTT 100 MOFs in the cyclopropanation reaction. Figure S11 shows that H3 could be efficiently recycled for at least four runs. The crystallinity of the H3 and the proportion of L_H in it are maintained, as shown in Figures S12 and S13 and Table S4. N₂ adsorption isotherms of reused H3 (Figure S14a) reveal that the surface area of the reused catalyst is lower than that of the fresh H3. This could be attributed to the decreased crystallinity and the formation of larger pores (Figure S14b) after repeated catalytic reactions.

4. CONCLUSIONS

The defect generating approach we provide in this work can tailor the catalytic properties of MOFs in two aspects simultaneously. Compared with the pristine MOFs, DE NOTT 100 MOFs present two unique features: (i) the protonated carboxylate groups as the Brønsted acid sites or the pyridyl N atoms as the Lewis basic sites are incorporated into the MOF frameworks, which can act as second active sites, and (ii) more modified PWs, which provide extra coordinatively unsaturated sites (CUSs), are generated. In summary, desired functional groups and modified metal nodes were successfully integrated into the NOTT 100 framework by partially substituting the parent linkers with defect generating linkers (L_H/L_{py}), thereby improving the catalytic performance of NOTT 100. Notably, the relative abundances of different types of defects (such as type I (modified node defects) and type II (missing node defects)) rely on the choice of defect generating ligands. However, due to the complex defect structure with two kinds of defect types and the presence of Lewis basic and Brønsted acidic additional sites influencing the catalytic properties, a quantitative correlation between different defects and their synergistical contribution to the catalytic performance is difficult to extract from our data so far. Such work is well beyond the scope of this study as it must be based on more precise structural and quantitative data on the abundance of various defects. Nevertheless, the concept of modulating the intrinsic (a weak) catalytic properties of pristine NOTT 100 by implementing specifically defect generating (truncated) linkers into the framework is further substantiated by our work.

AUTHOR INFORMATION

Corresponding Author

Roland A. Fischer – Chair of Inorganic and Metal Organic Chemistry, Department of Chemistry, Technical University of Munich, Garching 85748, Germany; orcid.org/0000 0002 7532 5286; Email: roland.fischer@tum.de

Authors

Zhiying Fan – Chair of Inorganic and Metal Organic Chemistry, Department of Chemistry, Technical University of Munich, Garching 85748, Germany

Junjun Wang – Institute of Functional Interfaces (IFG), Karlsruhe Institute of Technology, Eggenstein Leopoldshafen 76344, Germany

Weijia Wang – Institute of Functional Interfaces (IFG), Karlsruhe Institute of Technology, Eggenstein Leopoldshafen 76344, Germany; orcid.org/0000-0000-0003-0602-8162

Stefan Burger – Chair of Inorganic and Metal Organic Chemistry, Department of Chemistry, Technical University of Munich, Garching 85748, Germany

Zheng Wang – Chair of Inorganic and Metal Organic Chemistry, Department of Chemistry, Technical University of Munich, Garching 85748, Germany

Yuemin Wang – Institute of Functional Interfaces (IFG), Karlsruhe Institute of Technology, Eggenstein Leopoldshafen 76344, Germany; orcid.org/0000-0000-0002-9963-5473

Christof Wöll – Institute of Functional Interfaces (IFG), Karlsruhe Institute of Technology, Eggenstein Leopoldshafen 76344, Germany; orcid.org/0000-0000-0003-1078-3304

Mirza Cokoja – Chair of Inorganic and Metal Organic Chemistry, Department of Chemistry, Technical University of Munich, Garching 85748, Germany; orcid.org/0000-0000-3144-4678

Funding

This work is supported by German Research Foundation (DFG) project Fi 502/34 1 (DEMOFs).

Notes

The authors declare no competing financial interest.

[§]Former affiliation until December 2019.

ACKNOWLEDGMENTS

Z.F. and J.W. are grateful to the China Scholarship Council (CSC). S.B. would like to thank the Hanns Seidel Foundation for the financial support.

REFERENCES

- (1) Banerjee, R.; Phan, A.; Wang, B.; Knobler, C.; Furukawa, H.; O’Keeffe, M.; Yaghi, O. M. High throughput Synthesis of Zeolitic Imidazolate Frameworks and Application to CO₂ Capture. *Science* **2008**, *319*, 939–943.
- (2) Carter, J. H.; Han, X.; Moreau, F. Y.; da Silva, I.; Nevin, A.; Godfrey, H. G.; Tang, C. C.; Yang, S.; Schröder, M. Exceptional Adsorption and Binding of Sulfur Dioxide in a Robust Zirconium Based Metal–Organic Framework. *J. Am. Chem. Soc.* **2018**, *140*, 15564–15567.
- (3) Farha, O. K.; Yazaydin, A. Ö.; Eryazici, I.; Malliakas, C. D.; Hauser, B. G.; Kanatzidis, M. G.; Nguyen, S. T.; Snurr, R. Q.; Hupp, J. T. De novo Synthesis of a Metal–Organic Framework Material Featuring Ultrahigh Surface Area and Gas Storage Capacities. *Nat. Chem.* **2010**, *2*, 944–948.
- (4) Schneemann, A.; Bloch, E. D.; Henke, S.; Llewellyn, P. L.; Long, J. R.; Fischer, R. A. Influence of Solvent Like Sidechains on the Adsorption of Light Hydrocarbons in Metal–Organic Frameworks. *Chem. – Eur. J.* **2015**, *21*, 18764–18769.
- (5) Smith, G. L.; Eyley, J. E.; Han, X.; Zhang, X.; Li, J.; Jacques, N. M.; Godfrey, H. G. W.; Argent, S. P.; McPherson, L. J. M.; Teat, S. J.; Cheng, Y.; Frogley, M. D.; Cinque, G.; Day, S. J.; Tang, C. C.; Easun, T. L.; Rudić, S.; Ramirez Cuesta, A. J.; Yang, S.; Schröder, M. Reversible Coordinative Binding and Separation of Sulfur Dioxide in a Robust Metal–Organic Framework with Open Copper Sites. *Nat. Mater.* **2019**, *18*, 1358–1365.
- (6) Sumida, K.; Rogow, D. L.; Mason, J. A.; McDonald, T. M.; Bloch, E. D.; Herm, Z. R.; Bae, T. H.; Long, J. R. Carbon Dioxide Capture in Metal–Organic Frameworks. *Chem. Rev.* **2011**, *112*, 724–781.
- (7) Gascon, J.; Corma, A.; Kapteijn, F.; Llabrés i Xamena, F. X. Metal Organic Framework Catalysis: *Quo Vadis?* *ACS Catal.* **2013**, *4*, 361–378.
- (8) Farrusseng, D.; Aguado, S.; Pinel, C. Metal–Organic Frameworks: Opportunities for Catalysis. *Angew. Chem., Int. Ed.* **2009**, *48*, 7502–7513.
- (9) Corma, A.; García, H.; Llabrés i Xamena, F. X. Engineering Metal Organic Frameworks for Heterogeneous Catalysis. *Chem. Rev.* **2010**, *110*, 4606–4655.
- (10) Bavykina, A.; Kolobov, N.; Khan, I. S.; Bau, J. A.; Ramirez, A.; Gascon, J. Metal–Organic Frameworks in Heterogeneous Catalysis: Recent Progress, New Trends, and Future Perspectives. *Chem. Rev.* **2020**, DOI: 10.1021/acs.chemrev.9b00685.
- (11) Ding, M.; Flaig, R. W.; Jiang, H. L.; Yaghi, O. M. Carbon Capture and Conversion Using Metal–Organic Frameworks and MOF Based Materials. *Chem. Soc. Rev.* **2019**, *48*, 2783–2828.
- (12) Dhakshinamoorthy, A.; Li, Z.; Garcia, H. Catalysis and Photocatalysis by Metal Organic Frameworks. *Chem. Soc. Rev.* **2018**, *47*, 8134–8172.
- (13) Jiao, L.; Wang, Y.; Jiang, H. L.; Xu, Q. Metal–Organic Frameworks as Platforms for Catalytic Applications. *Adv. Mater.* **2018**, *30*, 1703663.
- (14) Horcajada, P.; Serre, C.; Vallet Regí, M.; Sebban, M.; Taulelle, F.; Férey, G. Metal–Organic Frameworks as Efficient Materials for Drug Delivery. *Angew. Chem., Int. Ed.* **2006**, *118*, 6120–6124.
- (15) Horcajada, P.; Chalati, T.; Serre, C.; Gillet, B.; Sebrie, C.; Baati, T.; Eubank, J. F.; Heurtaux, D.; Clayette, P.; Kreuz, C.; Chang, J. S.; Hwang, Y. K.; Marsaud, V.; Bories, P. N.; Cynober, L.; Gil, S.; Férey, G.; Couvreur, P.; Gref, R. Porous Metal–Organic Framework Nanoscale Carriers as a Potential Platform for Drug Delivery and Imaging. *Nat. Mater.* **2010**, *9*, 172–178.
- (16) Paz, F. A. A.; Klinowski, J.; Vilela, S. M. F.; Tomé, J. P. C.; Cavaleiro, J. A. S.; Rocha, J. Ligand Design for Functional Metal–Organic Frameworks. *Chem. Soc. Rev.* **2012**, *41*, 1088–1110.
- (17) Deria, P.; Mondloch, J. E.; Karagiari, O.; Bury, W.; Hupp, J. T.; Farha, O. K. Beyond Post Synthesis Modification: Evolution of Metal–Organic Frameworks via Building Block Replacement. *Chem. Soc. Rev.* **2014**, *43*, 5896–5912.
- (18) Burrows, A. D.; Frost, C. G.; Mahon, M. F.; Richardson, C. Post Synthetic Modification of Tagged Metal–Organic Frameworks. *Angew. Chem., Int. Ed.* **2008**, *120*, 8482–8614.
- (19) Cohen, S. M. Postsynthetic Methods for the Functionalization of Metal–Organic Frameworks. *Chem. Rev.* **2011**, *112*, 970–1000.
- (20) Erkartal, M.; Erkilic, U.; Tam, B.; Usta, H.; Yazaydin, O.; Hupp, J. T.; Farha, O. K.; Sen, U. From 2 Methylimidazole to 1,2,3 Triazole: A Topological Transformation of ZIF 8 and ZIF 67 by Post Synthetic Modification. *Chem. Commun.* **2017**, *53*, 2028–2031.
- (21) Fang, Z.; Dürholt, J. P.; Kauer, M.; Zhang, W.; Lochenie, C.; Jee, B.; Albada, B.; Metzler Nolte, N.; Pöppel, A.; Weber, B.; Muhler, M.; Wang, Y.; Schmid, R.; Fischer, R. A. Structural Complexity in Metal–Organic Frameworks: Simultaneous Modification of Open Metal Sites and Hierarchical Porosity by Systematic Doping with Defective Linkers. *J. Am. Chem. Soc.* **2014**, *136*, 9627–9636.
- (22) Erkartal, M.; Sen, U. Boronic Acid Moiety as Functional Defect in UiO 66 and Its Effect on Hydrogen Uptake Capacity and Selective CO₂ Adsorption: A Comparative Study. *ACS Appl. Mater. Interfaces* **2017**, *10*, 787–795.
- (23) Barin, G.; Krungleviciute, V.; Gutov, O.; Hupp, J. T.; Yildirim, T.; Farha, O. K. Defect Creation by Linker Fragmentation in Metal–Organic Frameworks and Its Effects on Gas Uptake Properties. *Inorg. Chem.* **2014**, *53*, 6914–6919.

- (24) Park, J.; Wang, Z. U.; Sun, L. B.; Chen, Y. P.; Zhou, H. C. Introduction of functionalized mesopores to metal–organic frameworks via metal–ligand–fragment coassembly. *J. Am. Chem. Soc.* **2012**, *134*, 20110–20116.
- (25) Fang, Z.; Bueken, B.; De Vos, D. E.; Fischer, R. A. Defect Engineered Metal–Organic Frameworks. *Angew. Chem., Int. Ed.* **2015**, *54*, 7234–7254.
- (26) Dissegna, S.; Epp, K.; Heinz, W. R.; Kieslich, G.; Fischer, R. A. Defective Metal Organic Frameworks. *Adv. Mater.* **2018**, *30*, 1704501.
- (27) Liu, L.; Chen, Z.; Wang, J.; Zhang, D.; Zhu, Y.; Ling, S.; Huang, K. W.; Belmabkhout, Y.; Adil, K.; Zhang, Y.; Slater, B.; Eddaoudi, M.; Han, Y. Imaging Defects and Their Evolution in a Metal–Organic Framework at Sub Unit Cell Resolution. *Nat. Chem.* **2019**, *11*, 622–628.
- (28) Cai, G.; Jiang, H. L. A Modulator Induced Defect Formation Strategy to Hierarchically Porous Metal–Organic Frameworks with High Stability. *Angew. Chem., Int. Ed.* **2017**, *56*, 563–567.
- (29) Yuan, S.; Zou, L.; Qin, J. S.; Li, J.; Huang, L.; Feng, L.; Wang, X.; Bosch, M.; Alsalmeh, A.; Cagin, T.; Zhou, H. C. Construction of Hierarchically Porous Metal–Organic Frameworks through Linker Labilization. *Nat. Commun.* **2017**, *8*, 15356.
- (30) Ji, P.; Drake, T.; Murakami, A.; Oliveres, P.; Skone, J. H.; Lin, W. Tuning Lewis Acidity of Metal–Organic Frameworks via Perfluorination of Bridging Ligands: Spectroscopic, Theoretical, and Catalytic Studies. *J. Am. Chem. Soc.* **2018**, *140*, 10553–10561.
- (31) Marx, S.; Kleist, W.; Baiker, A. Synthesis, Structural Properties, and Catalytic Behavior of Cu BTC and Mixed Linker Cu BTC PyDC in the Oxidation of Benzene Derivatives. *J. Catal.* **2011**, *281*, 76–87.
- (32) Kang, X.; Lyu, K.; Li, L.; Li, J.; Kimberley, L.; Wang, B.; Liu, L.; Cheng, Y.; Frogley, M.; Rudić, S.; Ramirez Cuesta, A. J.; Dryfe, R. A. W.; Han, B.; Yang, S.; Schröder, M. Integration of Mesopores and Crystal Defects in Metal Organic Frameworks via Templated Electrosynthesis. *Nat. Commun.* **2019**, *10*, 4466.
- (33) Kozachuk, O.; Luz, I.; Llabrés i Xamena, F. X.; Noei, H.; Kauer, M.; Albada, H. B.; Bloch, E. D.; Marler, B.; Wang, Y.; Muhler, M.; Fischer, R. A. Multifunctional, Defect Engineered Metal–Organic Frameworks with Ruthenium Centers: Sorption and Catalytic Properties. *Angew. Chem., Int. Ed.* **2014**, *53*, 7058–7062.
- (34) Zhang, W.; Kauer, M.; Halbherr, O.; Epp, K.; Guo, P.; Gonzalez, M. I.; Xiao, D. J.; Wiktor, C.; Llabrés i Xamena, F. X.; Wöll, C.; Fischer, R. A. Ruthenium Metal–Organic Frameworks with Different Defect Types: Influence on Porosity, Sorption, and Catalytic Properties. *Chem. – Eur. J.* **2016**, *22*, 14297–14307.
- (35) Zhang, W.; Kauer, M.; Guo, P.; Kunze, S.; Cwik, S.; Muhler, M.; Wang, Y.; Epp, K.; Kieslich, G.; Fischer, R. A. Impact of Synthesis Parameters on the Formation of Defects in HKUST 1. *Eur. J. Inorg. Chem.* **2017**, *2017*, 925–931.
- (36) Chen, B.; Ockwig, N. W.; Millward, A. R.; Contreras, D. S.; Yaghi, O. M. High H₂ Adsorption in a Microporous Metal–Organic Framework with Open Metal Sites. *Angew. Chem., Int. Ed.* **2005**, *44*, 4745–4749.
- (37) Lin, X.; Jia, J.; Zhao, X.; Thomas, K. M.; Blake, A. J.; Walker, G. S.; Champness, N. R.; Hubberstey, P.; Schröder, M. High H₂ Adsorption by Coordination Framework Materials. *Angew. Chem., Int. Ed.* **2006**, *45*, 7358–7364.
- (38) He, Y.; Zhou, W.; Yildirim, T.; Chen, B. A Series of Metal–Organic Frameworks with High Methane Uptake and an Empirical Equation for Predicting Methane Storage Capacity. *Energy Environ. Sci.* **2013**, *6*, 2735–2744.
- (39) Lin, X.; Telepeni, I.; Blake, A. J.; Dailly, A.; Brown, C. M.; Simmons, J. M.; Zoppi, M.; Walker, G. S.; Thomas, K. M.; Mays, T. J.; Hubberstey, P.; Champness, N. R.; Schröder, M. High Capacity Hydrogen Adsorption in Cu (II) Tetracarboxylate Framework Materials: The Role of Pore Size, Ligand Functionalization, and Exposed Metal Sites. *J. Am. Chem. Soc.* **2009**, *131*, 2159–2171.
- (40) Chang, X. H.; Qin, J. H.; Ma, L. F.; Wang, J. G.; Wang, L. Y. Two And Three Dimensional Divalent Metal Coordination Polymers Constructed from a New Tricarboxylate Linker and Dipyriddy Ligands. *Cryst. Growth Des.* **2012**, *12*, 4649–4657.
- (41) Pawley, G. S. Unit cell Refinement from Powder Diffraction Scans. *J. Appl. Crystallogr.* **1981**, *14*, 357–361.
- (42) Coelho, A. A. TOPAS and TOPAS Academic: An Optimization Program Integrating Computer Algebra and Crystallographic Objects Written in C++. *J. Appl. Crystallogr.* **2018**, *51*, 210–218.
- (43) Dissegna, S.; Vervoorts, P.; Hobday, C. L.; Düren, T.; Daisenberger, D.; Smith, A. J.; Fischer, R. A.; Kieslich, G. Tuning the Mechanical Response of Metal–Organic Frameworks by Defect Engineering. *J. Am. Chem. Soc.* **2018**, *140*, 11581–11584.
- (44) Rogge, S. M. J.; Wieme, J.; Vanduyfhuys, L.; Vandenbrande, S.; Maurin, G.; Verstraelen, T.; Waroquier, M.; Van Speybroeck, V. Thermodynamic Insight in the High Pressure Behavior of UiO 66: Effect of Linker Defects and Linker Expansion. *Chem. Mater.* **2016**, *28*, 5721–5732.
- (45) Feng, X.; Hajek, J.; Jena, H. S.; Wang, G.; Veerapandian, S. K.; Morent, R.; De Geyter, N.; Leyssens, K.; Hoffman, A. E. J.; Meynen, V.; Marquez, C.; De Vos, D. E.; Van Speybroeck, V.; Leus, K.; Van Der Voort, P. Engineering a Highly Defective Stable UiO 66 with Tunable Lewis Brønsted Acidity: The Role of the Hemilabile Linker. *J. Am. Chem. Soc.* **2020**, *142*, 3174–3183.
- (46) Dürholt, J. P.; Keupp, J.; Rochus, S. The Impact of Mesopores on the Mechanical Stability of HKUST 1: A Multiscale Investigation. *Eur. J. Inorg. Chem.* **2016**, *2016*, 4517–4523.
- (47) Shearer, G. C.; Vitillo, J. G.; Bordiga, S.; Svelle, S.; Olsbye, U.; Lillerud, K. P. Functionalizing the Defects: Postsynthetic Ligand Exchange in the Metal Organic Framework UiO 66. *Chem. Mater.* **2016**, *28*, 7190–7193.
- (48) Wöll, C. Structure and Chemical Properties of Oxide Nanoparticles Determined by Surface Ligand IR Spectroscopy. *ACS Catal.* **2019**, *10*, 168–176.
- (49) Petkov, P. S.; Vayssilov, G. N.; Liu, J.; Shekhan, O.; Wang, Y.; Wöll, C.; Heine, T. Defects in MOFs: A Thorough Characterization. *ChemPhysChem* **2012**, *13*, 2025–2029.
- (50) Wang, Z.; Sezen, H.; Liu, J.; Yang, C.; Roggenbuck, S. E.; Peikert, K.; Fröba, M.; Mavrandonakis, A.; Supronowicz, B.; Heine, T.; Gliemann, H.; Wöll, C. Tunable Coordinative Defects in UHM 3 Surface Mounted MOFs for Gas Adsorption and Separation: A Combined Experimental and Theoretical Study. *Micropor. Mesopor. Mater.* **2015**, *207*, 53–60.
- (51) Wang, W.; Sharapa, D. I.; Chandresh, A.; Nefedov, A.; Heißler, S.; Heinke, L.; Studt, F.; Wang, Y.; Wöll, C. Interplay of Electronic and Steric Effects to Yield Low Temperature CO Oxidation at Metal Single Sites in Defect Engineered HKUST 1. *Angew. Chem., Int. Ed.* **2020**, *59*, 10514–10518.
- (52) Bordiga, S.; Regli, L.; Bonino, F.; Groppo, E.; Lamberti, C.; Xiao, B.; Wheatley, P.; Morris, R.; Zecchina, A. Adsorption Properties of HKUST 1 toward Hydrogen and Other Small Molecules Monitored by IR. *Phys. Chem. Chem. Phys.* **2007**, *9*, 2676–2685.
- (53) Noei, H.; Amirjalayer, S.; Müller, M.; Zhang, X.; Schmid, R.; Muhler, M.; Fischer, R. A.; Wang, Y. Low Temperature CO Oxidation over Cu Based Metal–Organic Frameworks Monitored by using FTIR Spectroscopy. *ChemCatChem* **2012**, *4*, 755–759.
- (54) Lu, Y.; Miller, J. D. Carboxyl Stretching Vibrations of Spontaneously Adsorbed and LB Transferred Calcium Carboxylates as Determined by FTIR Internal Reflection Spectroscopy. *J. Colloid Interf. Sci.* **2002**, *256*, 41–52.
- (55) Nguyen, P. T. K.; Nguyen, H. T. D.; Nguyen, H. N.; Trickett, C. A.; Ton, Q. T.; Gutiérrez Puebla, E.; Monge, M. A.; Cordova, K. E.; Gándara, F. New Metal–Organic Frameworks for Chemical Fixation of CO₂. *ACS Appl. Mater. Interfaces* **2018**, *10*, 733–744.
- (56) Peterson, G. W.; Au, K.; Tovar, T. M.; Epps, T. H., III. Multivariate CuBTC Metal–Organic Framework with Enhanced Selectivity, Stability, Compatibility, and Processability. *Chem. Mater.* **2019**, *31*, 8459–8465.
- (57) Vimont, A.; Goupil, J. M.; Lavalley, J. C.; Daturi, M.; Surblé, S.; Serre, C.; Millange, F.; Férey, G.; Audebrand, N. Investigation of Acid Sites in a Zeotypic Giant Pores Chromium (III) Carboxylate. *J. Am. Chem. Soc.* **2006**, *128*, 3218–3227.

- (58) Hadjiivanov, K. I.; Vayssilov, G. N. Characterization of Oxide Surfaces and Zeolites by Carbon Monoxide as an IR Probe Molecule. *Adv. Catal.* **2002**, *47*, 307–511.
- (59) Reva, I. D.; Plokhotnichenko, A. M.; Radchenko, E. D.; Sheina, G. G.; Blagoi, Y. P. The IR Spectrum of Formic Acid in an Argon Matrix. *Spectrochim. Acta, Part A* **1994**, *50*, 1107–1111.
- (60) North, M.; Pasquale, R.; Young, C. Synthesis of Cyclic Carbonates from Epoxides and CO₂. *Green Chem.* **2010**, *12*, 1514–1539.
- (61) Lu, X. B.; Darensbourg, D. J. Cobalt Catalysts for the Coupling of CO₂ and Epoxides to Provide Polycarbonates and Cyclic Carbonates. *Chem. Soc. Rev.* **2012**, *41*, 1462–1484.
- (62) Li, J.; Ren, Y.; Jiang, H. Application of Metal Organic Framework Materials in the Chemical Fixation of Carbon Dioxide. *Prog. Chem.* **2019**, *31*, 1350–1361.
- (63) Liu, M.; Wang, X.; Jiang, Y.; Sun, J.; Arai, M. Hydrogen Bond Activation Strategy for Cyclic Carbonates Synthesis from Epoxides and CO₂: Current State of the Art of Catalyst Development and Reaction Analysis. *Catal. Rev.* **2019**, *61*, 214–269.
- (64) Pal, T. K.; De, D.; Bharadwaj, P. K. Metal–Organic Frameworks for the Chemical Fixation of CO₂ into Cyclic Carbonates. *Coord. Chem. Rev.* **2020**, *408*, 213173.
- (65) Zalomaeva, O. V.; Maksimchuk, N. V.; Chibiryaev, A. M.; Kovalenko, K. A.; Fedin, V. P.; Balzhinimaev, B. S. Synthesis of Cyclic Carbonates from Epoxides or Olefins and CO₂ Catalyzed by Metal Organic Frameworks and Quaternary Ammonium Salts. *J. Energy Chem.* **2013**, *22*, 130–135.
- (66) Li, P. Z.; Wang, X. J.; Liu, J.; Lim, J. S.; Zou, R.; Zhao, Y. A Triazole Containing Metal–Organic Framework as a Highly Effective and Substrate Size Dependent Catalyst for CO₂ Conversion. *J. Am. Chem. Soc.* **2016**, *138*, 2142–2145.
- (67) Gao, W. Y.; Chen, Y.; Niu, Y.; Williams, K.; Cash, L.; Perez, P. J.; Wojtas, L.; Cai, J.; Chen, Y. S.; Ma, S. Crystal Engineering of an NbO Topology Metal–Organic Framework for Chemical Fixation of CO₂ under Ambient Conditions. *Angew. Chem., Int. Ed.* **2014**, *53*, 2615–2619.
- (68) da Silva, L. P. Theoretical Study of the Ring Opening of Epoxides Catalyzed by Boronic Acids and Pyridinic Bases. *J. Phys. Chem. C* **2017**, *121*, 16300–16307.
- (69) Jagtap, S. R.; Raje, V. P.; Samant, S. D.; Bhanage, B. M. Silica Supported Polyvinyl Pyridine as a Highly Active Heterogeneous Base Catalyst for the Synthesis of Cyclic Carbonates from Carbon Dioxide and Epoxides. *J. Mol. Catal. A: Chem.* **2007**, *266*, 69–74.
- (70) Agarwal, R. A.; Gupta, A. K.; De, D. Flexible Zn MOF Exhibiting Selective CO₂ Adsorption and Efficient Lewis Acidic Catalytic Activity. *Cryst. Growth Des.* **2019**, *19*, 2010–2018.
- (71) Corma, A.; Iglesias, M.; Llabrés i Xamena, F. X.; Sánchez, F. Cu and Au Metal–Organic Frameworks Bridge the Gap Between Homogeneous and Heterogeneous Catalysts for Alkene Cyclopropanation Reactions. *Chem. – Eur. J.* **2010**, *16*, 9789–9795.
- (72) Sun, C.; Skorupskii, G.; Dou, J. H.; Wright, A. M.; Dincă, M. Reversible Metalation and Catalysis with a Scorpionate like Metallo ligand in a Metal–Organic Framework. *J. Am. Chem. Soc.* **2018**, *140*, 17394–17398.
- (73) Brenna, S.; Ardizzioia, G. A. Carbene Transfer and Carbene Insertion Reactions Catalyzed by a Mixed Ligand Copper (I) Complex. *Eur. J. Organ. Chem.* **2018**, *2018*, 3336–3342.
- (74) Epp, K.; Bueken, B.; Hofmann, B. J.; Cokoja, M.; Hemmer, K.; De Vos, D.; Fischer, R. A. Network Topology and Cavity Confinement Controlled Diastereoselectivity in Cyclopropanation Reactions Catalyzed by Porphyrin Based MOFs. *Catal. Sci. Technol.* **2019**, *9*, 6452–6459.
- (75) Verde Sesto, E.; Maya, E. M.; Lozano, Á. E.; de la Campa, J. G.; Sánchez, F.; Iglesias, M. Novel Efficient Catalysts Based on Imine Linked Mesoporous Polymers for Hydrogenation and Cyclopropanation Reactions. *J. Mater. Chem.* **2012**, *22*, 24637–24643.
- (76) Diaz Requejo, M. M.; Pérez, P. J.; Brookhart, M.; Templeton, J. L. Substituent Effects on the Reaction Rates of Copper Catalyzed Cyclopropanation and Aziridination of *Para* Substituted Styrenes. *Organometallics* **1997**, *16*, 4399–4402.
- (77) Fraile, J. M.; García, J. I.; Martínez Merino, V.; Mayoral, J. A.; Salvatella, L. Theoretical (DFT) Insights into the Mechanism of Copper Catalyzed Cyclopropanation Reactions. Implications for Enantioselective Catalysis. *J. Am. Chem. Soc.* **2001**, *123*, 7616–7625.
- (78) Dörwald, F. Z. *Metal Carbenes in Organic Synthesis*; John Wiley & Sons: 1999; 114
- (79) Doyle, M. P. Transition Metal Carbene Complexes: Diazodecomposition, Ylide, and Insertion. In *Comprehensive Organometallic Chemistry II*; Abel, E. W., Stone, F. G. A., Wilkinson, G., Eds.; Elsevier, 1995; *12*, 421–468.

Repository KITopen

Dies ist ein Postprint/begutachtetes Manuskript.

Empfohlene Zitierung:

Fan, Z.; Wang, J.; Wang, W.; Burger, S.; Wang, Z.; Wang, Y.; Wöll, C.; Cokoja, M.; Fischer, R. A.

[Defect Engineering of Copper Paddlewheel-Based Metal-Organic Frameworks of Type NOTT-100: Implementing Truncated Linkers and Its Effect on Catalytic Properties.](#)

2020. ACS applied materials & interfaces, 12.

doi: [10.5445/IR/1000124102](https://doi.org/10.5445/IR/1000124102)

Zitierung der Originalveröffentlichung:

Fan, Z.; Wang, J.; Wang, W.; Burger, S.; Wang, Z.; Wang, Y.; Wöll, C.; Cokoja, M.; Fischer, R. A.

[Defect Engineering of Copper Paddlewheel-Based Metal-Organic Frameworks of Type NOTT-100: Implementing Truncated Linkers and Its Effect on Catalytic Properties.](#)

2020. ACS applied materials & interfaces, 12 (34), 37993–38002.

doi: [10.1021/acsami.0c07249](https://doi.org/10.1021/acsami.0c07249)

Lizenzinformationen: [KITopen-Lizenz](#)